ELSEVIER

Journal of Nuclear Materials 313–316 (2003) 1221–1228

journal of nuclear materials

www.elsevier.com/locate/jnucmat

Modeling of ELM events and their effect on impurity enrichment

J. Hogan [a,*], R. Colchin [a], D. Coster [b], L. Baylor [a], M. Fenstermacher [c], M. Groth [c], M. Wade [a]

[a] *Oak Ridge National Laboratory, Fusion Energy Division, Oak Ridge, TN 37830, USA*
[b] *Max Planck Institut fur Plasmaphysik, Garching D-85748, Germany*
[c] *Lawrence Livermore National Laboratory, Livermore, CA 94551, USA*

Received 27 May 2002; accepted 12 September 2002

Abstract

Modeling of transient impurity transport during large ELMs is used to explore basic processes which may determine ELM-averaged enrichment. The b2-Eirene code (solps4), used for DIII-D geometry, suggests that a complex sequence can occur during an ELM cycle in which a transiently detached phase, with relatively low enrichment, can occur even under nominally attached conditions. A slower recovery phase then follows, in which the effect of induced scrape-off layer flows can increase in importance. The model results are compared with available fast time-scale measurements. The observed increased enrichment with higher Z is similar to trends in basic particle reflection properties. Neon recycling processes may thus introduce a significant history effect, as illustrated by analysis of continuous, unforced neon accumulation in a DIII-D discharge with a well-characterized operational history.

Keywords: Plasma-wall interactions; Divertor; Boundary plasma; Neon; Recycling; B2-EIRENE code

1. Introduction

The attractiveness of H-mode plasmas for attaining steady-state thermonuclear conditions depends on the relation between ELM benefits (relatively effective core impurity removal, especially of helium ash) and drawbacks (intense heat flux pulses). The present status of models for extrapolation is discussed in [1].

In DIII-D experiments, plenum impurity enrichment was seen to increase in the sequence helium, neon and argon; and also increased with mid-plane D_2 puffing relative to divertor D_2 puffing, under otherwise similar conditions [2]. Similar H-mode experiments on ASDEX Upgrade and on JET with the MkIIAP configuration report increased enrichment with higher Z, but no marked sensitivity of enrichment to the puffing location [3]. The interpretation of the DIII-D experiments is that mid-plane puffing induces a D^+ scrape-off layer (SOL) flow which increases divertor enrichment [2], but this is not the case in the ASDEX-Upgrade and JET MkIIAP experiments, where possible flow effects are reported to be smaller than divertor ambient recycling levels.

However, from the modeling perspective these experiments have differing and, in some cases, limited time resolution compared with that needed to evaluate ELM-influenced enrichment on a uniform basis. For example, the DIII-D enrichment experiments were carried out with type I ELMs with frequency f_{ELM} 50–60 Hz. Thus, while ELMS occurred at ~15 ms intervals, spectroscopic measurements used an integration time >100 ms, the response time of the species-sensitive plenum pressure gauges was ~50 ms and divertor thomson scattering measurements were made at 50 ms intervals. The

* Corresponding author. Tel.: +1-865 574 1349; fax: +1-865 574 1191.
E-mail address: hoganjt@ornl.gov (J. Hogan).

0022-3115/03/$ - see front matter
PII: S0022-3115(02)01520-9

reported enrichment in these experiments was averaged over several ELM events. Thus the aim of this modeling work is to delineate some basic processes which could be involved in the interpretation of future experiments with better resolution.

2. Simulation of ELM effect on enrichment

A multi-species version (deuterium, carbon, neon and helium ions) of the b2-Eirene code (solps4) [4], has been used to make a time-dependent calculation of ELM behavior under conditions similar to those of the DIII-D puff and pump experiments. Divertor puffing from the private flux region and mid-plane puffing from the outboard top of the machine, in a lower single null configuration, are compared in the simulations, with a D_2 puffing rate $\sim$100 T1s^{-1} ($\sim 6 \times 10^{21}$ particles s^{-1}) for each case. Neon is puffed from the private flux region in both cases. An effective albedo (95% recycling) is prescribed at the baffle entrance. An ELM event is modeled by enhancing the electron and ion radial thermal and particle diffusivities from their equilibrium values (1 and 0.2 m^2/s, respectively) by fivefold in the outer 20% of the normalized plasma radius, during a 100 μs interval, with such events recurring at a prescribed frequency 100 Hz in the modeling case considered. This model leads to an estimated pedestal energy loss of 3–10%. Only a rough estimate of the equivalent pedestal energy loss, for comparison with an experimental value, is available since the whole edge core region is not modeled. Experimental support for these assumptions is drawn from DIII-D measurements of ELM-triggered ECE emission bursts, which last 5–150 μs and originate from normalized radius $\rho/a \sim 0.78$ [5]. After the abrupt ELM event other aspects of transport are left unchanged in the simulation and subsequent evolution is determined solely by the underlying radial transport and recycling. Fig. 1(center) shows the calculated variation of $T_{e,div}$ during a simulated cycle of ELM behavior. There is a temperature crash just after ELM onset producing $T_{e,div} < 1$ eV and a detached strike point. Then a slow recovery ($\tau_{recovery} \sim 1/f_{ELM}$) occurs, with $T_{e,div}$ rising to the pre-ELM level. Comparing mid-plane and divertor puffing cases, a significant difference is observed in $T_{i,div}$ (Fig. 2(a) and (b)). In the divertor puffing case $T_{i,div}$ for both the inner and outer strike point locations is $\sim$30% lower than for the mid-plane case, due to larger local

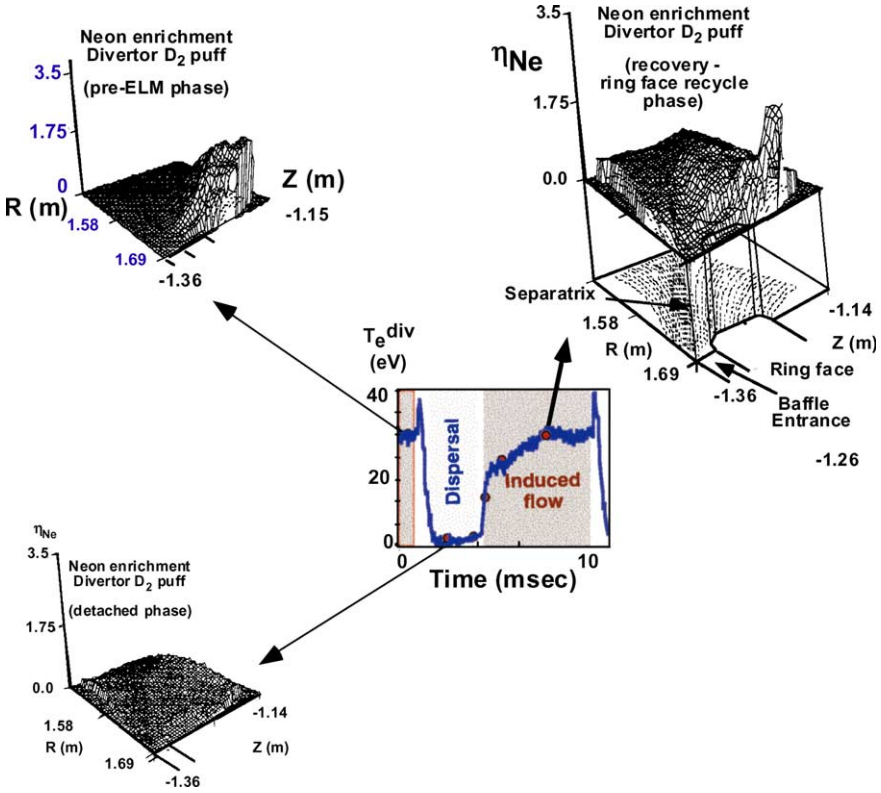

Fig. 1. One cycle of simulated ELM event showing $T_{e,div}$ evolution (center) and snapshots of neon enrichment spatial distributions (geometry at top right) at characteristic times during the ELM evolution.

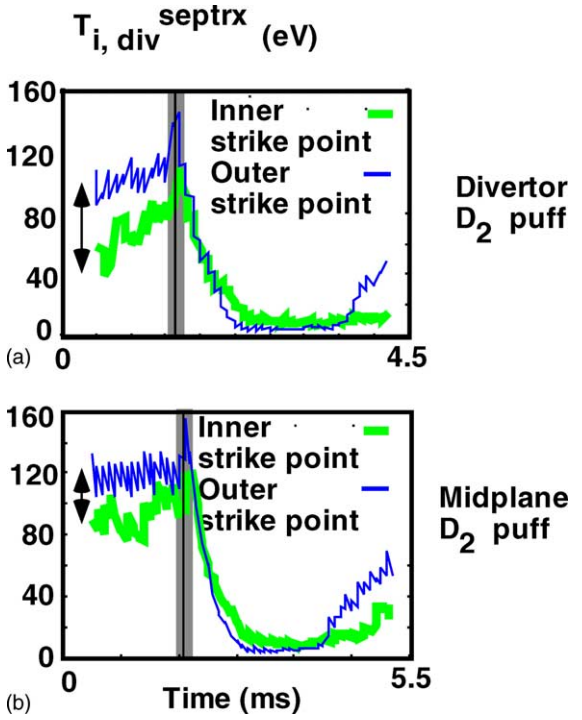

Fig. 2. $T_{i,div}$ evolution comparing mid-plane and divertor D_2 puffing cases.

deuterium charge exchange losses arising from the localized gas puff in the divertor. If this reduction held over the whole ELM cycle it would imply that the resulting reduction in the ion thermal force could be a more significant variable than induced SOL flow when comparing divertor and mid-plane puffing. However, as seen in Fig. 2(b), the difference in $T_{i,div}$ for the two cases narrows with the onset of the crash, and thereafter, during the recovery phase, $T_{i,div}$ is similar for both cases.

Fig. 1 further shows the evolution of the calculated neon enrichment profiles during the simulated ELM cycle. As a result of the reduced $T_{e,div}$ immediately after the ELM crash (transient detachment) the neon enrichment is sharply reduced, and then, as recovery of $T_{e,div}$ proceeds and neon is re-ionized after dispersal, enhanced neon recycling occurs at the outer face of the lower baffle ('ring face recycling'). The 'intra-ELM' recovery phase also allows a quiescent period for the operation of parallel flows in the SOL.

It should be noted that contrary behavior (i.e., attachment during ELM events and detachment intra-ELM) has been observed in ASDEX Upgrade for carbon during a density ramp [3]. However, the ELM detach-recovery sequence shown in the simulation would, *if* confirmed experimentally, have important implications for impurity enrichment. Fig. 3 shows a comparison in the poloidal plane between mid-plane and divertor puffing cases for the calculated parallel flow in the SOL of D^+ and low charge state neon ions during the recovery phase. For all neon ions there is an increased flow to the outer strike point (positive direction), leading to increased enrichment, for the mid-plane puffing case. Since there is strong variation in flow direction near the divertor plate, due to local recycling, these systematic increases can be difficult to see. A major effect of the induced SOL D^+ flow is to reduce accumulation at the inner strike point, thus increasing the neon density at the outer strike point and resulting in increased concentration. Note also, that although the difference in deuterium flow seems small in comparing divertor and mid-plane puffing cases, the absolute value of the local difference ($\sim 10^{22}$ pt/s) in the deuterium flow is be compared with the local change in the impurity flow ($\sim 3 \times 10^{14}$ pt/s).

Simulated time-resolved enrichment values are found to be 0.2 in the detached phase, 1.2–3.5 during the recovery phase, and 1.8 in the pre-ELM state, while the experimental ELM-averaged value is 2.3 for these conditions. For the same quantities in the divertor puffing case, simulated values are roughly half as large, in line with experimental findings. Thus, on the basis of the simulation, ELM-averaged enrichment is composed of contributions from strongly disparate phases (detachment and recovery) and the net enrichment depends on the balance between them. The relative strength of each phase, in turn, depends on core transport and instability processes (ELM magnitude and frequency) and thus must be found experimentally. A similar range of temporal variation in helium enrichment during ELM events has been seen in ASDEX Upgrade simulations [6]. While no complete time- and space-resolved measurements exist at present, some points of contact between the simulation and existing fast-time-scale measurements can be compared to assess model validity.

3. Comparison with available time-resolved data

By determining the relative time after the ELM temperature crash, some comparison can be made of the behavior during a single ELM cycle. Fig. 4(a) shows the D_α Type I ELM signature for a shot from the DIII-D enrichment study both in real time and referred to the relative phase within an ELM cycle. Fig. 4(b) shows the evolution of the Thomson scattering measurement of T_e in the divertor, for both cases. From Fig. 4(a) and (b) there shows the expected decrease in D_α following the ELM crash and also an upward trend (recovery) in $T_{e,div}$. However, measured enrichment behavior cannot show a clear dependence, owing to the long baffle and pressure gauge time constants.

A more direct comparison is possible for the fluxes to the baffle during an ELM event. The simulated time

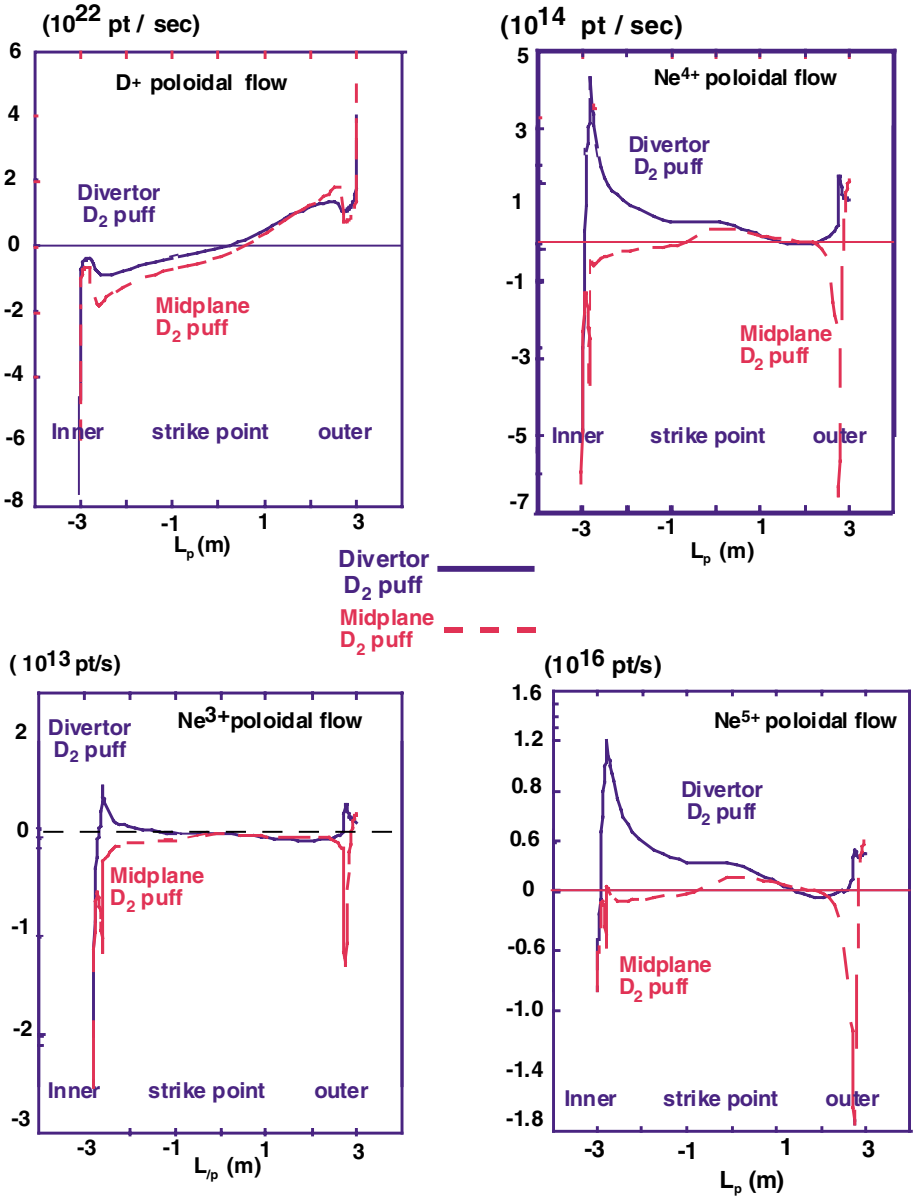

Fig. 3. Deuterium ion and selected neon ion flows in the SOL, comparing mid-plane and divertor puffing cases.

dependence of neon and deuterium fluxes to the baffle for the divertor D_2 puffing case is shown in Fig. 5(a). There is a predicted time shift between the arrival of peak D^+ flux and the neon flux, due to the slower parallel transport of the heavier neon ions in the SOL. In comparison, Fig. 5(b) shows the measured D_α and Ne I emission from an upper single null divertor discharge in DIII-D, both for the upper strike point and for the lower surface of the vessel. The emission is measured with an array of filter-scopes (see [7]) with high time-resolution. The frequency response (~10 kHz) is sufficient to discriminate the arrival of the D^+ and neon fluxes to the strike point. As seen in Fig. 5(b) the time shift between deuterium and neon fluxes seen in the simulation is also observed in this case.

One result of both the simulation and the data is that the enrichment is determined in an environment in which a high density of neutral deuterium can co-exist with low ionization-stage impurities. Increased attention should therefore be paid to the role of low energy charge exchange between D^0 and impurities, since at present, simulations use a species-insensitive scaling law for the

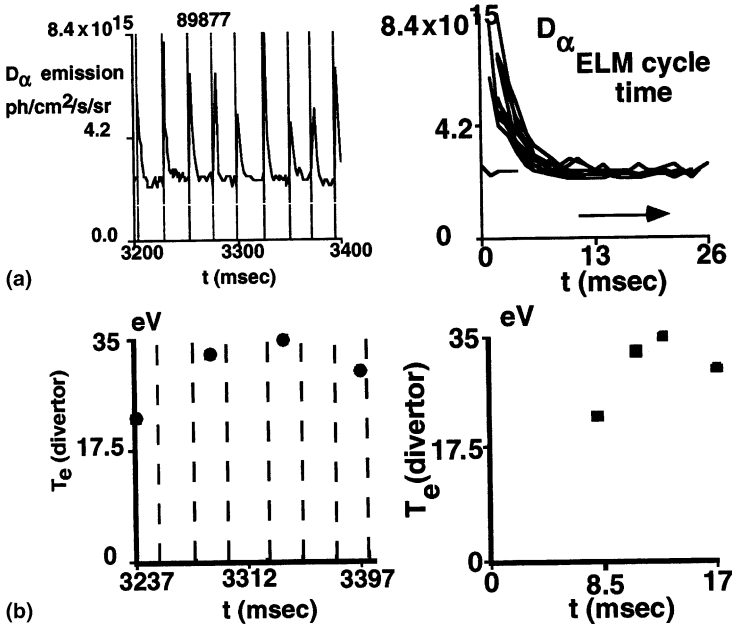

Fig. 4. (a) Simulation results for flux of D^+ and total neon ion density at the baffle entrance during and just after an ELM event. (b) Filter-scope chord-averaged measurements of the of D_α and Ne I emission during and just after an ELM event.

charge exchange rate ($R_{CX} = 2 \times 10^{-15} Z^{1.14} T_i^{0.35}$) [8]. Significant variation in both species- and charge state dependence is expected in the atomic physics.

The filter-scope array technique has the limitation that the emission is averaged over a chord length, so that higher time-resolution is achieved at the expense of local spatial resolution. Recently, a fast gated tangential viewing wavelength filtered camera system, which measures 2D spatial impurity distributions on the ELM time-scale, has been installed on DIII-D [9]. Preliminary indications (CIII emission) are encouraging as to future prospects for more detailed comparison of simulation and experiment [10] and the testing of ELM models.

4. Relation of surface processes to enrichment trends

In DIII-D ELM-averaged enrichment is found to increase in the series of cases helium, neon, argon and, unlike the dependence on puffing location, this trend is also seen in the ASDEX-Upgrade [11] and JET MkII AP experiments [12].

Alternatives to neo-classical flow effects may thus be involved. One such is related to basic surface reflection properties. For reference, taken from Table 1 in [2], typical values of ELM-averaged enrichment in DIII-D for mid-plane/divertor puffing cases are: helium (1.1/0.9), neon (2.3/1.2) and argon (17/6), In comparison, representative values for the normal incidence reflected energy probability at an incident (sheath) energy of 50 eV on a pure carbon target, obtained from TRIM code results [13], are He^+ (0.2), Ne^+ (0.03) and Ar^+ (0.004), an order of magnitude decrease with each case. One might expect that the enrichment increases as the average mean free path of energetic reflected particles decreases, and that the increase in enrichment with increased Z could plausibly result from a strong reduction in reflected particle fraction. Time- and wavelength-resolved spectroscopic measurements near the divertor plates during the ELM cycle would help in resolving the issue.

Analysis, along these lines, of neon penetration experiments for L- and RI-mode discharges in TEXTOR-94 [14], led to the conclusion that a much higher fraction of fast reflected neon atoms was observed than could be expected on the basis of simple application of TRIM results for a pure carbon surface. Eirene analysis showed that a significant increase in reflection particle fraction and energy (compared with TRIM values) was required to fit the spectroscopic data. The authors noted that implantation of neon in the target could increase the effective mass of the target material and thus give rise to such an increased reflection probability.

Support for this interpretation can be inferred from DIII-D experiments. Fig. 6 shows the evolution of neon density in a discharge with isolated Type I ELMs. As can be seen, there is a steady increase in the core neon content, with a step increase at each ELM event. The discharge shown in Fig. 6 was one of the first discharges of the day with injected neutral beam power, but there

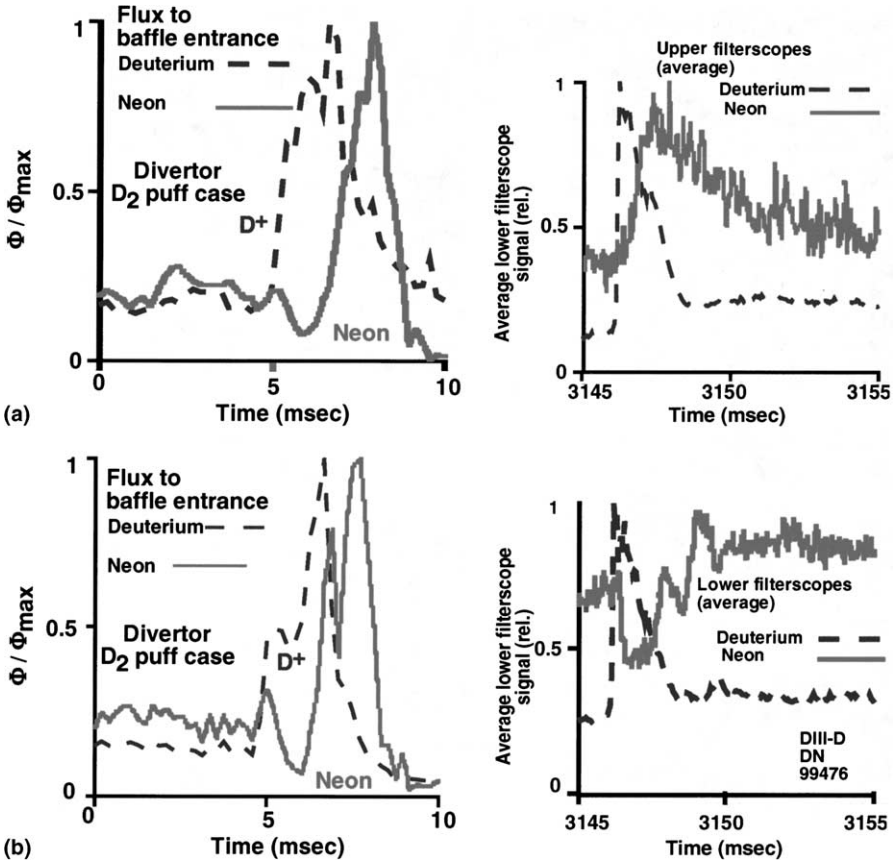

Fig. 5. (a) D_α emission for DIII-D lower single null discharge with giant ELMs (both real time and time relative to ELM event). (b) Measured electron temperature in divertor region (both real time and time relative to ELM event).

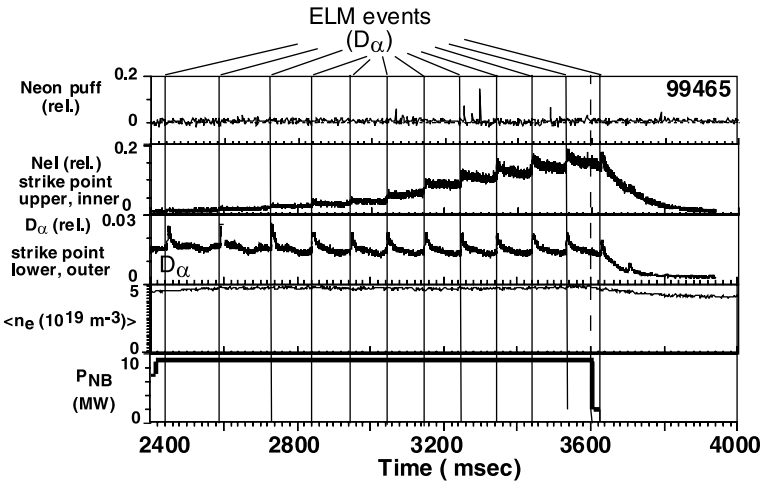

Fig. 6. Discharge showing steady neon increase without prior neon injection: neon puff signal (~0), lower, outer strike point D_α emission, Ne I emission from upper inner strike point, average electron density, beam power.

was no neon injection in this discharge, nor in any preceding discharges on that day. On the preceding day of operations, however, strong neon puffing was done in 25 out of 34 discharges.

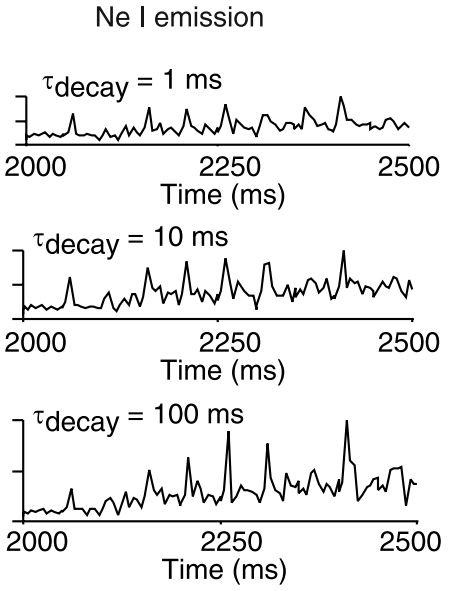

Fig. 7. Simulation (MIST) of the evolution of Ne I emission due solely to ELM-stimulated neon release, for assumptions $\tau_{decay} = 1$, 10, 100 ms. Trend for rising neon accumulation seen as τ_{decay} increases.

In order to assess the possibility of neon accumulation without injection, the MIST radial impurity transport code [15] with an explicit ELM model [16] has been used in a heuristic simulation of a characteristic discharge. A multi-reservoir model, similar to that described in [17], balances the total core, divertor and plenum neon content and the exchanges between these reservoirs. The neon influx is modeled as $\Gamma_{Ne} = \eta_{Ne}\Gamma_{D^+}$, that is, a neon source due only to deuterium impact. Typical measured fast D_α signals fix the time of the ELM crash, τ_{ELM}, and the recycling decay time, τ_{decay}, $\Gamma_{D^+} = \Gamma_D^+(\tau_{ELM})\ e^{-(t-\tau_{ELM})/\tau_{decay}}$. Characteristic values $\tau_{plenum} = 0.04$ s, $\tau_{div} = 0.7$ s and $\tau_{plenum\text{-}div} = 0.1$ s are used to describe the inter-reservoir exchanges in the calculation. Fig. 7 shows predicted Ne I emission for several assumed values of τ_{decay}. The neon source in the calculation arises only from impact due to the ELM-induced D^+ flux, and steadily rising neon content is found for these cases with the (ad hoc) neon 'sputtering' coefficient $\eta_{Ne} = 0.005$. Thus neon accumulation *without* neon injection is simulated, suggesting the importance of a wall source of neon which can be liberated by ELMs. Ion-induced desorption is a candidate process which could reproduce the trends found in this empirical simulation.

5. Discussion and conclusions

Modeling of impurity density evolution during type I ELM events shows that ELM-averaged enrichment in the DIII-D case considered has several distinct phases during the ELM cycle: transient detachment with low enrichment, followed by recovery with effect both of flows (increasing enrichment) and of local recycling (decreasing enrichment). Extrapolation of enrichment values to future burning plasma experiments requires an assessment as to which phase will dominate. Support for the impurity dynamics treatment in the model is found in comparison with fast filter-scope spectroscopic diagnostics. Further validation of the model though comparison with time- and space-resolved data, which is now becoming available, is clearly desirable.

The improved treatment of particle drifts available in the later solps5 version of b2-Eirene would be needed to make a more detailed comparison of the flow rates with theory, but here the simpler aim has been to delineate the phases in the ELM process when flows are important compared with the large convective processes in an ELM event. On the basis of the modeling, several factors may be identified for the resolution of reported differences in enrichment behavior. Better characterization of the ELM frequency and amplitude, development of local neutral density measurements in the divertor, and improved (species-sensitive) atomic data for deuterium-impurity charge exchange are required.

Finally, direct evidence has been found for the role of ELMs in removing previously implanted impurities. ELM-induced evolution of neon is observed to arise from the divertor plates and wall, in a case without neon injection, and global modeling suggests that ELM impact provides a mechanism to liberate the previously trapped neon. This suggests that any extrapolation to future steady state, or long pulse, scenarios using extrinsic impurity injection to increase radiative losses or to mitigate ELM effects must also include a validated wall balance model for the retention of the extrinsic impurities.

Acknowledgements

The B2-Eirene code is provided by the B2-Eirene development group: R. Schneider, D. Coster, X. Bonnin (IPP-Garching, Greifswald) and D. Reiter, P. Boerner (FZ-Juelich). This research was sponsored in part by the Office of Fusion Energy Sciences, US Department of Energy, under contract DE-AC05-00OR22725 with Oak Ridge National Laboratory managed by UT-Battelle, LLC.

References

[1] A. Loarte, J. Nucl. Mater. 290–293 (2001) 805;
A.S. Kukushkin, G. Janeschitz, A. Loarte, et al., J. Nucl. Mater. 290–293 (2001) 887.

[2] M. Wade, R. Wood, S. Allen, et al., J. Nucl. Mater. 266–269 (1999) 44.
[3] H.-S. Bosch, Plasma Phys. Control. Fusion 8 (1999) 401.
[4] R. Schneider et al., J. Nucl. Mater. 196–198 (1992) 810.
[5] Ch. Fuchs, M. Austin, Phys. Plasmas 5 (2001) 1594.
[6] D. Coster, H.-S. Bosch, W. Ullrich, et al., J. Nucl. Mater. 290–293 (2001) 845.
[7] R. Isler, R. Colchin, N. Brooks, et al., Plasma Phys. 8 (2001) 4470.
[8] M.E. Piuatti et al., Plasma Phys. 23 (1981) 1075.
[9] M. Groth et al., these Proceedings.
[10] M. Fenstermacher, M. Groth, C. Lasnier, et al., Bull. Am. Phys. Soc. 46 (2001) 225.
[11] H.-S. Bosch, W. Ullrich, D. Coster, et al., J. Nucl. Mater. 290–293 (2001) 836.
[12] M. Groth, P. Andrew, W. Fundamenski, et al., J. Nucl. Mater. 290–293 (2001) 867.
[13] W. Eckstein, IPP-Report 9/117, Association Euratom-IPP, Garching, Germany, 1998.
[14] B. Unterberg, H. Knauf, P. Bogen, et al., J. Nucl. Mater. 220–222 (1995) 462.
[15] R. Hulse, Fusion Technol. 3 (1983) 259.
[16] J. Hogan, M. Wade, M. Schaffer, et al., Europhys. Conf. Abstracts, V22C, 1998, p. 834.
[17] R. Dux, A. Kallenbach, M. Bessenrodt-Weberpals, et al., Plasma Phys. Control. Fusion 38 (1996) 989.